IMPACT OF CONVERTER EQUIVALENT IMPEDANCE ON DISTANCE PROTECTION WITH THE MHO CHARACTERISTIC

Shuxiu Cao[1], Qiteng Hong[1], Di Liu[1], Liang Ji[2], Campbell Booth[1]*

[1]*Department of Electronic and Electrical Engineering, University of Strathclyde, Glasgow, United Kingdom*
[2]*College of Electrical Engineering, Shanghai University of Electric Power, Shanghai, China*
**q.hong@strath.ac.uk*

Keywords: CONVERTER EQUIVALENT IMPEDANCE, MHO CHARACTERISTICS, DISTANCE PROTECTION, MEMORY POLARISATION, CONVERTER-DOMINATED POWER SYSTEMS

Abstract

With the rapid increase of Converter-Based Resources (CBRs) and the decommission of conventional Synchronous Generators (SGs), recent studies have found that distance protection can face significant challenges. One of the key factors that can impact the protection performance is the CBRs' fault behaviour being different from SGs, leading to the different characteristics of their equivalent internal impedance, which will have a particular impact on distance protection with the memory-polarised Mho characteristic. This paper presents a comprehensive investigation of the characteristics of the equivalent internal impedance of CBRs with different control strategies, based on which, their impact on the memory-polarised Mho distance protection is analysed in detail. In the paper, the equivalent impedance of CBRs with virtual impedance-based Grid Forming Control (GFM) and balanced current injection-based Grid Following Control (GFL) are calculated and plotted against time throughout the faults. These are then compared with the internal impedance of a reference voltage source. It is found that, unlike the SGs, which can be considered as voltage sources and have constant source impedance, CBRs' internal impedance have dynamic and time-varying characteristics, which are governed by the implemented Fault-Ride-Through (FRT) control strategies. Such characteristics will lead to dynamical changes in the expansion levels of the Mho protection zones, which could lead to increase risks of protection failure and/or maloperation. It is also revealed that, by better understanding the internal impedance characteristics of CBRs, the control strategies of CBRs could potentially be refined to mitigate the negative impact on Mho distance operation, thus presenting a potential solution to mitigate the risks of compromised performance of memory-polarised Mho distance protection.

1 Introduction

Modern power systems are experiencing a rapid increase of renewable generation to promote low-carbon and sustainable energy development [1]. Renewable resources are typically interfaced with the network via power electronics converters, so Converter-Based Resources (CBRs) will gradually replace Synchronous Generators (SGs), and power systems are expected to evolve from SGs to CBRs dominated systems. Conventional protection schemes were developed based on the assumption that the fault currents are mainly contributed by SGs [2]. However, the massive integration of CBRs, along with their diverse control strategies used, has led to significant changes in fault characteristics compared with conventional SG-dominated systems. For CBRs, the control schemes deployed determine the characteristics of the voltage and current during faults, which are typically governed by the Grid Codes (GCs) [3]. These unconventional fault characteristics of CBRs can introduce unprecedented challenges for conventional protection systems [4].

Distance protection is extensively applied in transmission systems [5]. Recent studies have found that, the different fault behaviour of CBRs (e.g. fault current magnitude, phase, etc.) can introduce significant risks of compromised performance in distance protection [6]. As reported in [7], for certain converter control modes (e.g. balanced current control), there could be oscillations in the measured impedance locus, resulting in a refuse-to-trip failure in distance protection. In [8], it is found that there is a large phase difference between fault currents at both ends of the protected line connecting with CBRs, leading to impedance measurement errors and potential false tripping in distance protection. Due to the different voltage and current characteristics, the equivalent internal impedance of CBRs will also be significantly different from conventional SGs, which are typically considered as voltage sources with constant internal impedance. This will have a particular impact on distance protection with the memory-polarised Mho characteristic.

The research reported in [9] investigates the risk of maloperation of memory-polarised Mho distance protection in CBR-dominated power systems, where their unpredictable characteristics of the dynamical changes in the Mho protection zone were highlighted. In [10], the impact of P-Q controlled Photo-Voltaic (PV) generators on positive-sequence memory-polarised Mho distance protection is presented, where it was found that the reliability of the Mho distance protection operation may be compromised. To explore the adaptive Mho characteristic of distance protection, [11] presents a uniform expression of the adaptive setting

impedance of distance protection, in order to adaptively adjust the Mho protection zone for the correct identification of internal and external faults. While the aforementioned studies have presented valuable findings of the Mho distance protection performance in CBR-dominated networks, the characteristic of the equivalent impedance of CBRs, particularly when different control strategies are deployed, has not been well understood. As a result, there is limited understanding of the fundamental mechanism of the impact of CBRs with different control strategies on the operation of Mho distance protection.

There are various research activities, focusing on dynamic characteristics modelling of the equivalent internal impedance of CBRs, in order to support protection operations. [12] proposes an adaptive distance protection algorithm that calculates positive and negative-sequence PV source impedances via the Thevenin Equivalent (TE) theorem of using the local measurement data, subsequently modifying the quadrilateral characteristic of the distance relay based on these calculated equivalent source impedances. In [13], the CBR is equivalent to a fixed voltage source with a variable series impedance. Using the pure-fault sequence network from this equivalent model, the sequence fault current angles are calculated to precisely identify the fault type.

These publications provide valuable insights on how the internal impedance of CBRs can be characterised and represented, but they do not investigate how the dynamically changed internal impedance of CBRs can impact Mho distance protection. This paper therefore aims to address the aforementioned technical gaps by presenting a comprehensive investigation of the characteristics of the equivalent internal impedance of CBRs with different control strategies, based on which, their impact on the memory-polarised Mho distance protection is analysed in detail. In the paper, the equivalent impedance of CBRs with virtual impedance-based Grid Forming Control (GFM) and balanced current injection-based Grid Following Control (GFL) are calculated and visualised throughout the fault period and compared with the internal impedance of a reference voltage source. With a better understanding of the internal impedance characteristics of CBRs, it is expected that the control strategies of CBRs could potentially be refined to mitigate the negative impact on Mho distance operation, thus presenting a potential solution to mitigate the risks of compromised performance of distance protection with the memory-polarised Mho characteristic.

The rest of the paper is organised as follows: Section 2 introduces the basic principle of distance protection with the Mho characteristic; Section 3 introduces the calculation method of the equivalent impedance of CBRs; Section 4 investigates the equivalent internal impedance of CBRs with different control strategies and analyses the impact on the memory-polarised Mho distance protection; conclusions of the paper and future work are presented in Section 5.

2 Mho Characteristic of Distance Protection

Distance relays work by assessing the apparent impedance utilising local voltage and current measurements, based on which, it will identify whether there is a fault and whether the fault is within the predefined protection zone. Therefore, the precise measurement of apparent impedance is critical for the correct operation of distance relays. Distance relays typically consist of two impedance measurement groups, i.e. one for phase-to-ground (AG, BG, CG elements) and the other for phase-to-phase (AB, BC, CA elements). The expressions for all impedance measurement elements can be found in [14].

According to the operating principle, the Mho distance element is typically divided into three types: self-polarised, crossed-polarised and memory-polarised Mho elements. To avoid inaccuracy in impedance measurement during close-in faults, memory polarisation is widely used [9]. It works by using a phase angle comparator between an operating quantity and a polarising quantity for fault identifications and tripping decisions makings.

Fig. 1 and Fig. 2 illustrate a simplified model of a transmission line connected with CBRs and the basic principle of the memory-polarised Mho element respectively. As shown in Fig. 2, the operation of a memory-polarised Mho element achieved via a phase comparator with two inputs, i.e. S_1 and S_2, which are defined as follows:

$$\begin{cases} S_1 = V_r + pV_{mem} \\ S_2 = V_r - Z_r I_r \end{cases} \tag{1}$$

where, V_r and I_r are the voltage and current measured by the distance relay, p is the polarising factor; V_{mem} is the memory-polarised voltage; and Z_r is the zone reach of the distance relay, which is set as 0.8 Z_{1L} in this paper (i.e. zone-1 reach).

V_{mem} is the pre-fault memory voltage, and as reported in [15], i.e. $V_{mem} = V_s = V_r + Z_s I_r$. Accordingly, (1) can be simplified as

$$\begin{cases} S_1 = \dfrac{V_r}{I_r} + \dfrac{p}{1+p} Z_S \\ S_2 = \dfrac{V_r}{I_r} - Z_r \end{cases} \tag{2}$$

The absolute value of the angle between S_1 and S_2, i.e. θ, is considered as the criterion for fault identifications and tripping decisions, which is described as (3)-(4).

$$\theta = \left|\arg(S_1) - \arg(S_2)\right| \tag{3}$$

$$\begin{cases} 0^\circ \le \theta < 90^\circ & \text{no-trip} \\ 90^\circ \le \theta \le 180^\circ & \text{trip} \end{cases} \tag{4}$$

As shown in Fig.2, the memory-polarised Mho element has an additional benefit that the expanded protection zone will provide larger resistive reach. However, the operation principle is based on the following two assumptions [16]: 1) the source impedance magnitude behind the relay point is constant and predictable, facilitating accurate calculation of the additional resistive reach; 2) the voltage phase angle remains nearly constant during faults, enabling the estimation of the short-circuit voltage's phase angle from the pre-fault voltage (referred to the memory voltage). While these assumptions are valid in SG-dominated power systems, these might not be applicable in CBR-dominated systems. As

discussed previously, the equivalent internal impedance of CBRs can vary during faults and is dependent on the CBR's control. Therefore, it is critical to understand the dynamic features of CBR's equivalent impedance, in order to better understand the fundamental mechanism of how the control will impact Mho distance protection operation, thus informing effective solutions to address them.

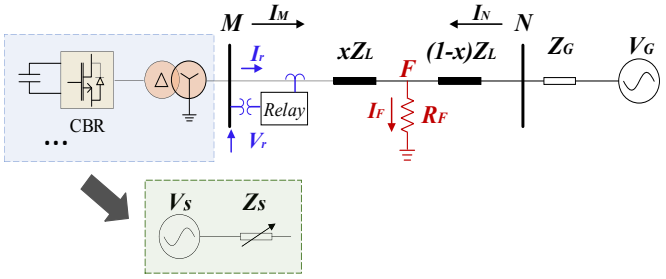

Fig. 1 Simplified model of a transmission line connected with CBRs

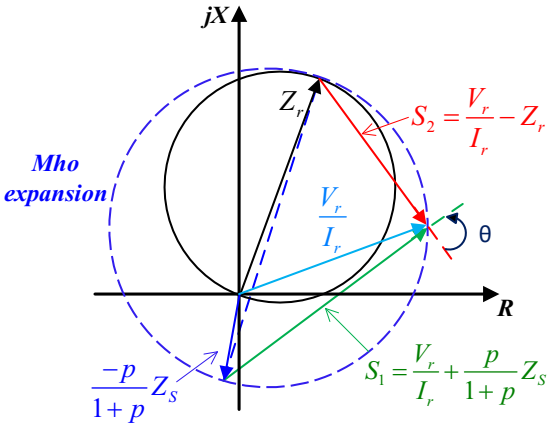

Fig. 2 Basic principle of the memory-polarised Mho element

3 Characterisation of CBR's Equivalent Impedance

As shown in Fig. 1, assuming the CBR under investigation is connected to a grid dominated by SGs, the grid side can be represented by a voltage source (i.e. V_G) connected in series with a fixed equivalent impedance (i.e. Z_G). It should be noted that, this might not be true for a grid dominated by CBRs, but as the focus of the paper is placed on the CBR connected to the left-hand side, so the above assumption is used for simplicity. In accordance with the TE theorem, an equivalent voltage source (i.e. V_S) with a variable series impedance (i.e. Z_S) can be used for representing the CBR being studied.

With such a representation of an equivalent voltage source and a variable series impedance, the positive-sequence, negative-sequence and zero-sequence equivalent networks for the system in Fig. 1 can be presented as Fig. 3, where the sequence networks can be connected flexibly to represent different fault scenarios (e.g., connected in series with single-phase-to-ground faults). However, since the positive-sequence, negative-sequence and zero-sequence equivalent impedances of CBR in their individual networks are analysed and calculated respectively, which is not affected by the relevant connecting relations between the sequence networks. Therefore, the sequence networks in Fig.3 have not been connected, in order to represent a general condition. The equation calculating the positive-sequence, negative-sequence and zero-sequence equivalent impedances of CBR is presented in (5), which is derived by applying the Kirchhoff's Voltage Law (KVL) to the left circuit of the busbar M in the following individual sequence networks.

$$\begin{cases} Z_{1S} = \dfrac{V_S - V_{1r}}{I_{1r}} \\ Z_{2S} = -\dfrac{V_{2r}}{I_{2r}} \\ Z_{0S} = -\dfrac{V_{0r}}{I_{0r}} \end{cases} \tag{5}$$

where, V_S is the equivalent voltage source of CBR; the components in the positive, negative and zero-sequence networks are indicated by the subscripts of '1', '2' and '0'.

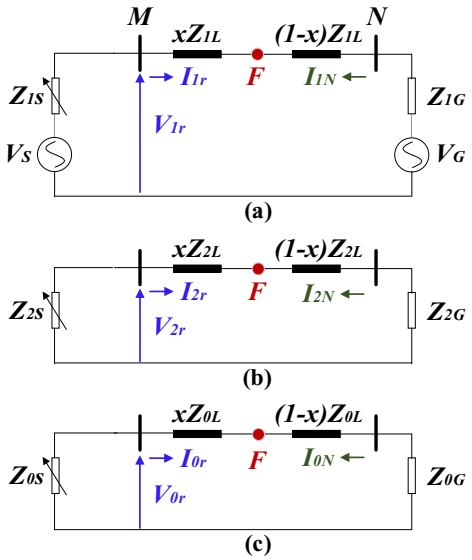

Fig. 3 General sequence network of the system in Fig. 1: (a) positive-sequence network; (b) negative-sequence network; (c) zero-sequence network

4 Evaluation of CBR's Equivalent Impedance and its Impacts on the Mho Characteristic

4.1 Overview of the test system

This section presents a comprehensive investigation of the characteristics of the equivalent internal impedance of CBRs with different control strategies, based on which, their impact on the memory-polarised Mho distance protection is analysed in detail. The schematic of the test system is shown in Fig. 4. Three cases are investigated: 1) a fixed voltage source along with constant series impedance is used as a reference case; 2) the fault infeed from one end is a GFL converter that uses balanced current injection-based control [17]; 3) the converter control strategy is replaced by the virtual impedance-based GFM control strategy [18]. Table 1 shows the parameters of the test system, and settings of the distance protection are provided in Table 2.

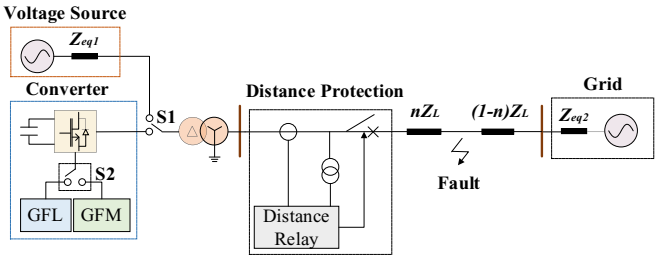

Fig. 4 Schematic of the test system

Table 1 Parameters of the test system

Parameters	Description	Values
V_s	Nominal system voltage (kV)	275
P_s	Converter rated capacity (MVA)	500
L	Protected line length (km)	12.1
K_v, K_c	Voltage/Current Transformer (CT/VT) rations	2500:1, 1200:1
R_1, R_0	Per-unit positive/zero-sequence resistance (Ω/km)	0.0378, 0.159
L_1, L_0	Per-unit positive/zero-sequence inductance (mH/km)	1.324, 3.202
C_1, C_0	Per-unit positive/zero-sequence capacitance (nF/km)	8.964, 6.48

Table 2 Settings of the distance relay

Parameter Description	Relay Settings
Protection characteristic	Positive-sequence memory-polarised Mho
Reach setting	Zone 1: 80%, Zone 2: 120%
Residual compensation factor	$K_0 = 0.48\angle -6.4°$
Time delay	Zone 1: 0 ms, Zone 2: 400 ms
Polarising factor	$p = 0.5$

Table 3 Studied cases with different fault conditions

Case	Fault conditions	The investigated cases
1	5 Ω, 15%, AG, SCR=3	These fault conditions are tested in all the investigated cases, i.e. voltage source, GFL control, and GFM control.
2	5 Ω, 50%, AG, SCR=3	
3	5 Ω, 15%, BC, SCR=3	
4	5 Ω, 15%, ABC, SCR=3	
5	5 Ω, 15%, AG, SCR=7	

4.2 Simulation results and analysis

To evaluate the impact of GFL and GFM control strategies on the equivalent impedances of CBRs in the events of different faults, a group of the cases, as shown in Table 3, are analysed in details. It should be noted that, the fault period is set as 0.20s-0.34s. Furthermore, the results shown in Fig.5 (a)-(f) (i.e. results of case 1) are used as a reference group.

4.2.1 Different fault locations: As shown in Fig. 5, in terms of AG fault with different fault locations, the positive-sequence equivalent impedance of the voltage source is same to its negative-sequence equivalent impedance, which is consistent with the source internal impedance of voltage source that has been configured in simulation. In addition, the calculated zero impedance of the voltage source is small as it is solidly grounded, which is similar to the observations with the connection of GFL and GFM. In Fig.5 (a) and (b), the dynamical changes in the positive-sequence equivalent impedances of CBR with GFL control appear to be more significant than with GFM control, where AG fault is located on 15% of the protected line. However, in the case of AG fault on the 50% of the protected line, there is a similar trend of the dynamical changes in the positive-sequence equivalent impedances of CBRs using the GFL and GFM control strategies. Also, values of the angle of these positive-sequence equivalent impedances would increase when the fault location is progressively away from the CBR side. Furthermore, the magnitude of the negative-sequence equivalent impedance of CBR with GFL control is significantly high because there are no negative sequence currents being injected during faults, which results in the open circuit in the negative-sequence network at the converter side. As it can be seen that, for AG fault, the positive-sequence equivalent impedance is not equal to the negative-sequence equivalent impedance in either control strategy.

4.2.2 Different fault types: In the presence of BC fault in case 3, both positive-sequence equivalent impedances of CBRs with GFL and GFM control are different from their negative-sequence equivalent impedances, which is aligned with the observation in the AG fault in case 1. Furthermore, the magnitudes and angles of positive and negative-sequence equivalent impedances in case 3 are close to the values in case 1. However, for the ABC fault in case 4, the magnitudes and angles of positive-sequence equivalent impedance is larger, compared to the results in case 1. In terms of positive-sequence equivalent impedances, a similar trend can be observed from magnitudes and angles.

4.2.3 Different Short Circuit Ratios (SCRs): As shown in Fig. 7, the dynamical changes in the positive-sequence equivalent impedances of CBR with GFL control are more significant than with GFM control, when the SCR of the test system is changed from 7 to 2. In case 5, the magnitude and angle of the positive-sequence equivalent impedance of CBR with GFL control is larger than the results in case 1. Compared with all of the tested cases with different fault conditions, it is found that, the dynamical changes in CBR's equivalent impedance are sensitive to the changes of the system SCRs.

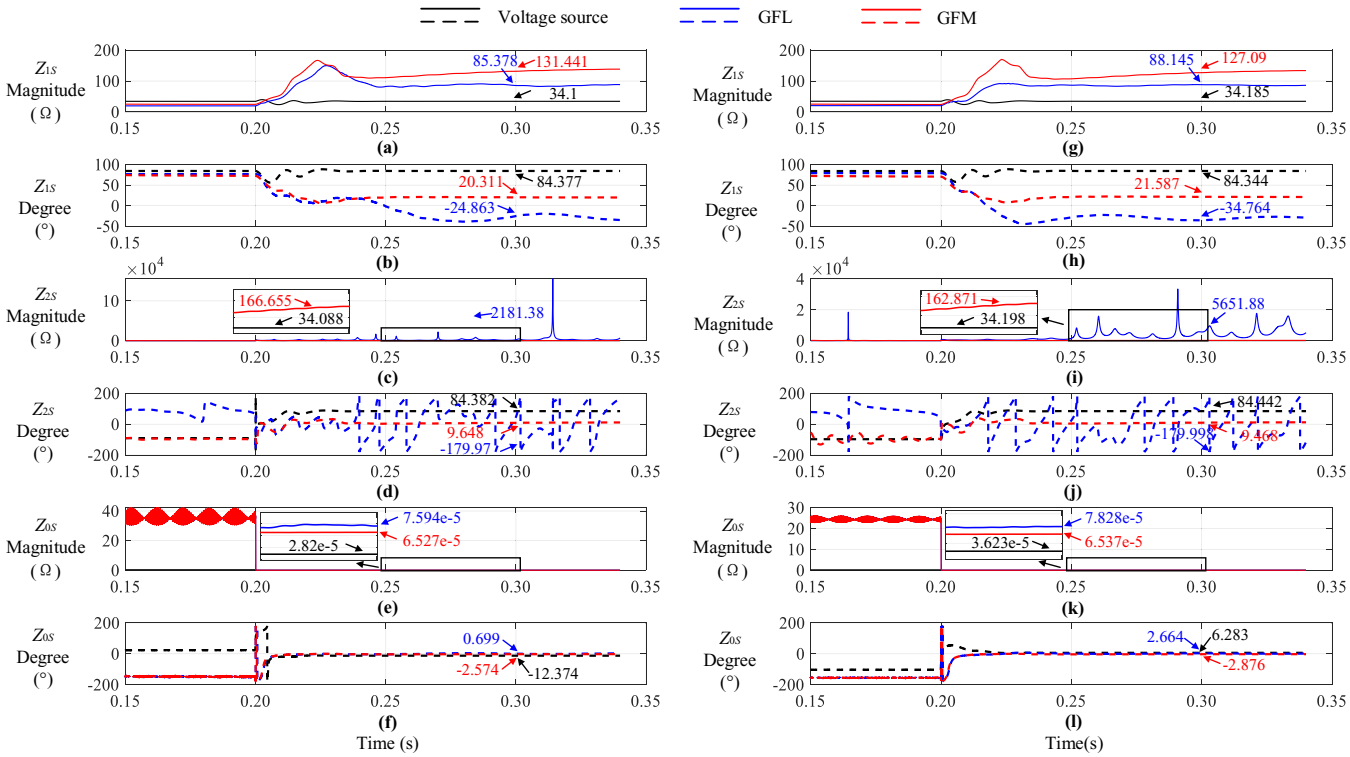

Fig. 5 The equivalent impedance of CBRs and voltage source for case 1 (i.e. (a)-(f)) and case 2 (i.e. (g)-(h))

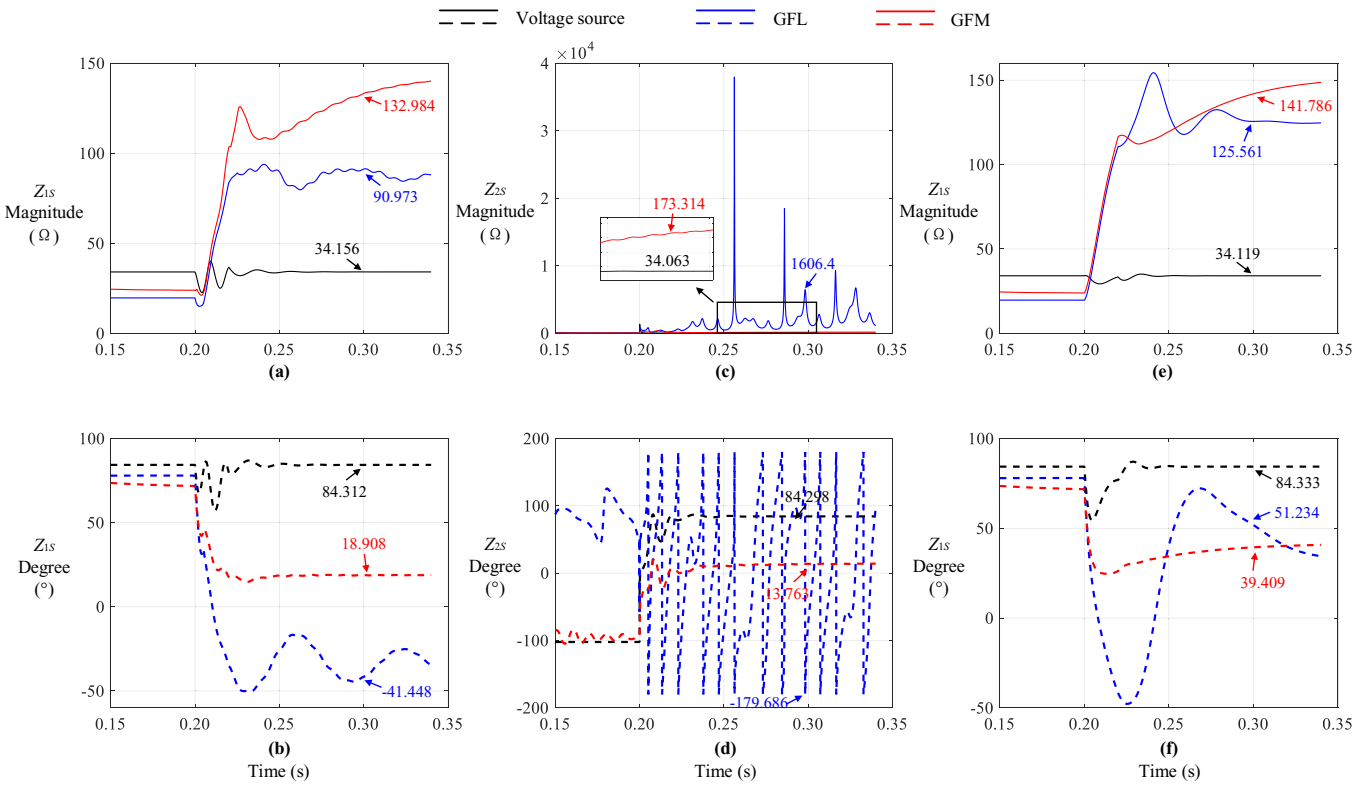

Fig. 6 The equivalent impedance of CBRs and voltage source for case 3 (i.e. (a)-(d)) and case 4 (i.e. (e)-(f))

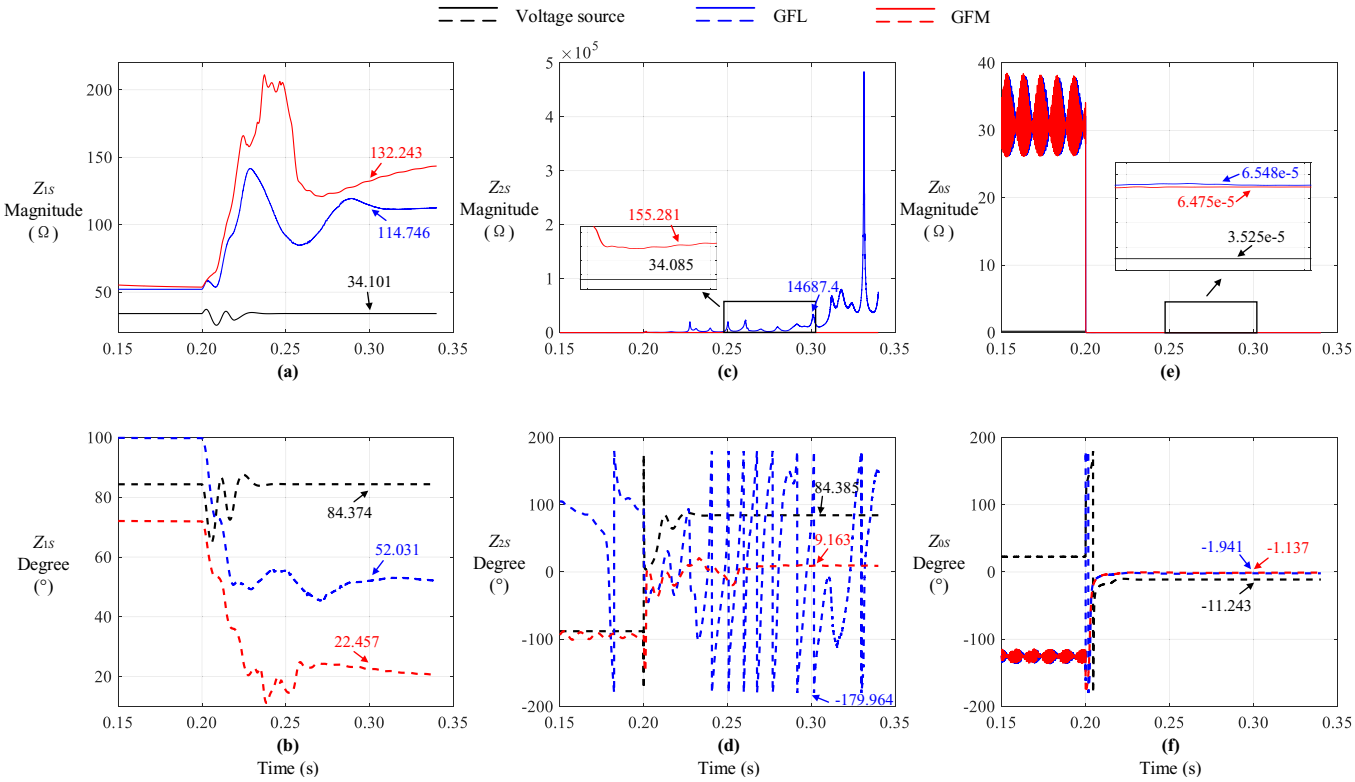

Fig. 7 The equivalent impedance of CBRs and voltage source for case 5

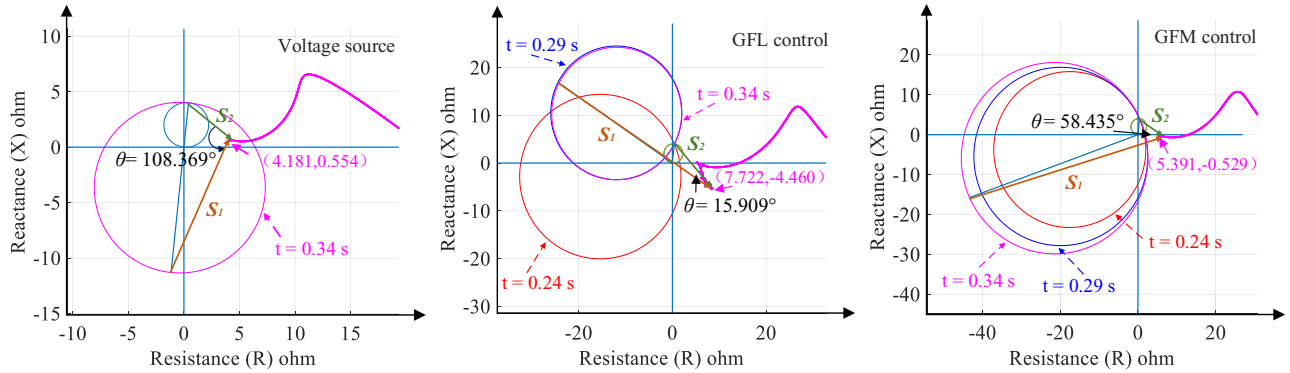

Fig. 8 Dynamical changes in the Mho protection zones of (a) case I, (b) case II and (c) case III

4.2.4 Impact of the equivalent impedance of CBRs on the dynamical changes in the Mho protection zones: To evaluate this, as shown in Table 4, a group of the cases are analysed in details as follows.

Table 4 Studied cases in the test system

Cases	The investigated cases in the test system	Fault conditions
I	Voltage source	5 Ω, 15%, AG SCR=3
II	GFL	
III	GFM	

It should be noted that, it is assumed that the distance protection with the positive sequence memory-polarised Mho characteristic is used in the test system, where the following cases only take the positive-sequence equivalent impedances of CBRs and voltage source into account.

For case I, there is no dynamical change in the Mho protection zone due to the voltage source with the constant source impedance. As shown in Fig. 8 (a), the measured impedance locus is located at the boundary of the Mho protection zone considering the additional polarising input (i.e. $\frac{-p}{1+p}Z_{1S}$). The measured angle (i.e. θ) of the phase comparator with two inputs, i.e. S_1 and S_2, is larger than 90°, so the distance protection can correctly operate. For Case II, with progressive time after fault occurrence, the Mho protection zones increasingly expand towards the third quadrant, and then move to the second quadrant. However, it is shown in Fig. 8 (b) that, the measured impedance locus is apparently beyond the Mho protection zone border, and the measured value of θ is less than 90°. Therefore, the dynamic

characteristics of the equivalent impedances of CBR with GFL control would lead to increase risks of distance protection failure. Similarly, considering the equivalent impedance characteristics of CBR with GFM control, the measured impedance locus in case III is located beyond the Mho protection zone, and the measured value of θ is also less than 90°, resulting in the failure of distance protection.

5 Conclusion

In this paper, a comprehensive investigation of the characteristics of the equivalent internal impedance of CBRs with different control strategies is presented, based on which, their impact on the memory-polarised Mho distance protection is analysed in detail. In the paper, the equivalent impedance of CBRs with virtual impedance-based GFM and balanced current injection-based GFL are calculated using the TE theorem, which are then compared with the internal impedance of a voltage source. It is found that, different from SGs, which can be considered voltage sources and have constant source impedance, CBRs' internal impedances has dynamic and time-varying characteristics, which are governed by the different FRT control strategies implemented. Such characteristics will lead to the dynamical changes in the Mho protection zones, which could lead to increase risks of protection failure and/or maloperation. It is also revealed that, by better understanding the internal impedance characteristics of CBRs, the control strategies of CBRs could potentially be refined so as to mitigate the negative impact on Mho distance operation, thus presenting a potential desirable solution to mitigate the risks of compromised performance of distance protection with the memory-polarised Mho characteristic.

6 Acknowledgements

The research is jointly supported by the University of Strathclyde Student Excellence Award (SEA) and EPSRC RESCUE project (EP/T021829/1).

7 References

[1] Henninger, S., Jaeger, J.: 'Advanced classification of converter control concepts for integration in electrical power systems', Int. J. Electr. Power Energy Syst., 2020, 123, pp 1-14

[2] Banaiemoqadam, A., Hooshyar, A., Azzouz, M. A.: 'A control-based solution for distance protection of lines connected to converter-interfaced sources during asymmetrical faults', IEEE Trans. Power Del., 2020, 35, (3), pp 1455-1466

[3] Azzouz, M. A., Hooshyar, A.: 'Dual current control of inverter-interfaced renewable energy sources for precise phase selection', IEEE Trans. Smart Grid, 2019, 10, (5), pp 5092-5102

[4] Cao, S., Hong, Q., Liu, D., et al.: 'Review and evaluation of control-based protection solutions for converter-dominated power systems', 2023 IEEE Belgrade PowerTech, Belgrade, Serbia, Jun 2023, pp 1-7

[5] Ma, J., Xiang, X., Li, P., et al.: 'Adaptive distance protection scheme with quadrilateral characteristic for extremely high-voltage/ultra-high-voltage transmission line', IET Gen., Trans., Dist., 2017, 11, (7), pp 1624-1633

[6] Paladhi, S., Pradhan, A. K.: 'Adaptive distance protection for lines connecting converter-interfaced renewable plants', IEEE J. Emerg. Sel. Topics Power Electr., 2021, 9, (6), pp 7088-7098

[7] Jia. J., Yang. G., Nielsen, A. H., et al.: 'Impact of VSC control strategies and incorporation of synchronous condensers on distance protection under unbalanced faults', IEEE Trans. Ind. Electron., 2019, 66, (2), pp 1108-1118

[8] Haddadi, A., Kocar, I., Mahseredjian, J., et al.: 'Negative sequence quantities-based protection under inverter-based resources challenges and impact of the German grid code', Electr. Power Energy Syst., 2020, 188, pp 1-6

[9] Haddadi, A., Zhao, M., Kocar, I., et al.: 'Impact of inverter-based resources on memory-polarised distance and directional protective relay elements', 2020 52nd North American Power Symposium, Arizona, USA, Apr 2021, pp 1-6

[10] Radhakrishnan, A., Priyamvada, I. R. S., Das, S.: 'Impact of P–Q control based PV generator on memory-polarised Mho relay', 2022 International Conference on Smart Energy Systems and Technologies, Eindhoven, Netherlands, Sep 2022, pp 1-6

[11] Liang, Y., Li, W., Zha, W.: 'Adaptive mho characteristic-based distance protection for lines emanating from photovoltaic power plants under unbalanced faults', IEEE Syst. J., 2020, 15, (3), pp 3506-3516

[12] Mishra, P., Pradhan, A. K., Bajpai, P.: 'Adaptive distance relaying for distribution lines connecting inverter-interfaced solar PV plant', IEEE Trans. Ind. Electron., 2020, 68, (3), pp 2300-2309

[13] Paladhi, S., Pradhan, A. K.: 'Adaptive fault type classification for transmission network connecting converter-interfaced renewable plants', IEEE Syst. J., 2020, 15, (3), pp 4025-4036

[14] Kasztenny, B., Finney, D.: 'Fundamentals of Distance Protection', 2008 61st Annual Conference for Protective Relay Engineers, Texas, USA, Apr 2008, pp 1-34

[15] Liu, D., Hong, Q., Dyśko, A., et al.: 'Hardware-in-the-loop tests and analysis of HVDC system's impact on distance protection performance', The 17th International Conference on AC and DC Power Transmission, Online, Dec 2021, pp 1-6

[16] El-Arroudi, K., Joós, G.: 'Performance of interconnection protection based on distance relaying for wind power distributed generation', IEEE Trans. Power Del., 2018, 33, (2), pp 620-629

[17] Liu, D., Hong, Q., Dyśko, A., et al.: 'Evaluation of HVDC system's impact and quantification of synchronous compensation for distance protection', IET Renew. Power Gen., 2022, 16, (9), pp 1-16

[18] Rosso, R., Engelken, S., Liserre, M.: 'On the implementation of an FRT strategy for grid-forming converters under symmetrical and asymmetrical grid faults', IEEE Trans. Ind. Appl., 2021, 57, (5), pp 4385-4397